Progress in Reaction Kinetics and Mechanism

ARTICLE

Open Access

https://doi.org/10.48130/prkm-0025-0011

Progress in Reaction Kinetics and Mechanism **2025**, 50: e010

Synthesis and photocatalytic performance of g-C_3N_4-CuO-ZnO for efficient degradation of crystal violet (CV) and methyl orange (MO) dyes under sunlight irradiation

Sidra Pervaiz[1], Muhammad Saeed[1*], Mohamed A. Habila[2], Muhammad Asghar Jamal[1], Atta ul Haq[1], Iltaf Khan[3] and Mohsin Javed[4]

[1] *Department of Chemistry, Government College University Faisalabad, Faisalabad 38000, Pakistan*
[2] *Department of Chemistry, College of Science, King Saud University, P.O Box 2455, Riyadh 11451, Saudi Arabia*
[3] *School of Chemical Science and Engineering, Tongji University, Shanghai 200092, China*
[4] *Department of Chemistry, Quaid-i-Azam University, Islamabad 45320, Pakistan*
* Corresponding author, E-mail: msaeed@gcuf.edu.pk

Abstract

In the present study, a g-C_3N_4-CuO-ZnO heterojunction was successfully synthesized using a cost-effective co-precipitation method and evaluated for its photocatalytic efficiency in degrading crystal violet (CV) and methyl orange (MO) dyes under sunlight irradiation. Comprehensive characterization through XRD, FTIR, SEM, and TGA confirmed the successful formation of the heterojunction, revealing enhanced structural, morphological, and thermal properties. Photocatalytic performance studies showed remarkable degradation efficiencies of 99.26% for CV and 96.84% for MO within 180 min, significantly outperforming individual g-C_3N_4, CuO, and ZnO catalysts. The optimized conditions—including pH, catalyst dosage, and reaction kinetics—highlighted the robustness and adaptability of the synthesized catalyst. The superior performance is attributed to the separation and reduction in recombination of electrons and holes, driven by an S-scheme charge transfer mechanism. These findings demonstrate the potential of g-C_3N_4-CuO-ZnO as an effective and sustainable catalyst for tackling dyes in wastewater, offering a promising avenue for environmental remediation.

Citation: Pervaiz S, Saeed M, Habila Mohamed A, Jamal MA, Haq A, et al. 2025. Synthesis and photocatalytic performance of g-C_3N_4-CuO-ZnO for efficient degradation of crystal violet (CV) and methyl orange (MO) dyes under sunlight irradiation. *Progress in Reaction Kinetics and Mechanism* 50: e010 https://doi.org/10.48130/prkm-0025-0011

Introduction

Water and air are the most essential requirements for human survival. The industrial development and increase in population have led to numerous environmental complications such as water contamination, air pollution, and soil contamination due to solid waste such as plastics, which threatens a clean and healthy environment. As a result, the deterioration of the environment is more severe than its expectations[1–4]. The industries that contribute significantly to water pollution include paper and pulp, textile, tannery, and pharmaceutical industries. Synthetic dyes are the main industrial pollutants that are most difficult to eliminate from the environment. Due to high stability, these dyes pose serious environmental challenges[5,6]. A wide range of protocols have been reported for the eradication of dyes from wastewater. These techniques include reverse osmosis, membrane separation, chemical precipitation, adsorption, ion exchange, chemical and biological decomposition, aerobic/anaerobic digestion, and photocatalysis[7–10]. The photocatalytic process, a light-driven process, has recently gained significant attention from researchers for the treatment of organic pollutants containing wastewater due to its effectiveness in mineralizing pollutants. One key advantage of photocatalysis is its ability to degrade a broad spectrum of contaminants, including those resistant to other treatment methods[11]. Additionally, it is preferred over alternative techniques for its superior performance, minimal generation of secondary pollutants, cost-effectiveness, ease of operation, and environmental friendliness. Photocatalysis involves the generation of reactive species that contribute significantly to this process, facilitating the conversion of toxic pollutants into harmless substances[12–16]. ZnO is a transition metal oxide that is used for many applications[17]. ZnO is widely used as a catalyst in photodegradation of organic pollutants. However, despite its effectiveness as a photocatalyst, its photocatalytic activity is not high due to relatively wide band gap energy (3.2 eV). A desirable photocatalyst is one that is capable of absorbing both ultraviolet and visible radiation, as solar radiation consists of approximately 45% visible light and less than 10% ultraviolet light, along with other forms of radiation. As sunlight is a renewable source of energy, therefore the development of solar light-driven photocatalytic systems is highly desirable[18–20]. A number of procedures have been reported for addressing these limitations and boosting the photocatalytic activity of ZnO[21–25]. The development of photocatalysts by combination of different materials is one of the techniques that enhances the catalytic activity through the improvement of light-harvesting capability of the catalysts. The combination of ZnO with a semiconductor of narrow bandgap energy such as CuO (band gap 1.4 eV) produces a photocatalyst that effectively absorbs the visible spectrum of incident light and enables the electron transfer to ZnO. Although copper oxide (CuO) has a narrow bandgap substance, allowing for effective visible light absorption, its activity is not appreciable due to the recombination of the photo-induced charges. However, the p-n heterojunction formed by coupling a p-type CuO with an n-type ZnO facilitates the reverse transport of carriers, reducing recombination, and extending their lifetime. However, the overall photocatalytic performance is still significantly limited due to poor absorption and utilization of light[26,27]. It has been reported that effectiveness and stability of the catalysts can be enhanced by combining metal oxides with C-based substances such as g-C_3N_4, graphene

oxide, or CNTs. Particularly, the g-C_3N_4 is a promising substrate for the improvement in catalytic performance of a number of oxides. Graphitic carbon nitride (g-C_3N_4), which is a polymeric substance comprised of repeating tris-triazine units, has got significant interest in the field of photocatalysis. Its relatively small bandgap (~2.7 eV) enables a swift response in the visible light region, making it highly effective for solar light absorption[28]. With optimal band structure, excellent stability, simple, and cost-effective synthesis methods, and an environmentally friendly nature, g-C_3N_4 is regarded as a versatile material. The combination of g-C3N4 with metal oxides increases the active sites resulting in improved catalytic performance[29–34].

This work is focused on the synthesis of g-C_3N_4-CuO-ZnO heterojunction photocatalyst for the efficient degradation of crystal violet (CV) and methyl orange (MO) dyes in aqueous solutions.

Experimentation

Chemicals

The chemicals used include urea [NH_2CONH_2] (99%) purchased from Merck, copper nitrate trihydrate [$Cu(NO_3)_2{\cdot}3H_2O$] (99%), and zinc nitrate hexahydrate [$Zn(NO_3)_2{\cdot}6H_2O$] (99%) purchased from SRL, polyvinyl alcohol [PVA] (99%) purchased from Qualigens, and sodium hydroxide pellets [NaOH] (99%) purchased from Rankem.

Synthesis g-C_3N_4-CuO-ZnO

g-C_3N_4-CuO-ZnO heterojunction was prepared in two steps. In the first step, g-C_3N_4 was prepared by calcining the urea. Typically, 10 g urea was put in muffle furnace and heated to 550 °C at 5°C per min. It was kept at 550 °C for 3 h. Then it was cooled to room temperature naturally. After grinding, a yellow color g-C_3N_4 powder was obtained and was used for further investigation.

In the second step, g-C_3N_4 was used for the synthesis of g-C_3N_4-CuO-ZnO. Typically, 5 g g-C_3N_4, 4.792 g $Zn(NO_3)_2{\cdot}6H_2O$, 0.6856 g $Cu(NO_3)_2{\cdot}3H_2O$, and 0.60 g PVA were added in 50 mL distilled water and stirred continuously for 30 min. Then, 1 M NaOH solution was added dropwise to the resultant suspension under continuous stirring till pH 10. After stirring for 3 h, the obtained precipitation was filtered and washed. After washing, it was dried at 100 °C overnight. The obtained solid was crushed into fine powder using mortar and pestle and calcined at 550 °C.

Characterization

The fabricated g-C_3N_4-CuO-ZnO was examined with XRD, FTIR, SEM, and TGA techniques. The Bruker D8 X-ray diffractometer, Hitachi S-4800 scanning electron microscope, Shimadzu FTIR 8400S spectrometer, and PerkinElmer TGA 8000 Thermogravimetric Analyzer were used for XRD, FTIR, SEM, and TGA, respectively.

Assessment of photocatalytic performance

The photocatalytic performance was assessed through the degradation of crystal violet and methyl orange dyes under sunlight irradiation using g-C_3N_4-CuO-ZnO as a catalyst. In a typical procedure, 50 mL of either dye solution was placed in a beaker, and 0.05 g g-C_3N_4-CuO-ZnO was added to it. The adsorption-desorption equilibrium was ensured by stirring the mixture for 30 min in the dark. After this period, a sample was collected and analyzed. Subsequently, the reaction mixture was exposed to sunlight with continuous stirring, and samples were taken at regular intervals for analysis with a UV-visible spectrophotometer.

Reaction kinetics

Heterogeneous catalytic reactions are generally described by the Langmuir-Hinshelwood mechanism. The present study is also a heterogeneous reaction hence it can also be described by the Langmuir-Hinshelwood mechanism. Accordingly, the g-C_3N_4-CuO-ZnO catalyzed degradation of crystal violet/methyl orange dye proceeds in the following steps[35–37].

1. Adsorption of MO/CY on g-C_3N_4-CuO-ZnO;
2. Harvesting of sunlight;
3. Degradation of dye(s) molecules.

Therefore, the rate of reaction can be expressed as:

$$Rate = -\frac{C_{dye}}{dt} \propto Irradiation\ C_{dye} \tag{1}$$

As the reaction mixture is continuously irradiated, therefore it becomes independent of irradiation. Hence,

$$Rate = -\frac{dC_{dye}}{dt} = kC_{dye} \tag{2}$$

$$Rate = -\frac{dC_{dye}}{C_{dye}} = kt \tag{3}$$

On integration

$$-\int_{(C_{dye})0}^{(C_{dye})t} \frac{dC_{dye}}{C_{dye}} = k\int_0^t dt \tag{4}$$

$$ln\frac{[C_{dye}]_o}{[C_{dye}]_t} = kt \tag{5}$$

Taking anti log, we get:

$$\frac{[C_{dye}]_o}{[C_{dye}]_t} = e^{kt} \tag{6}$$

$$\frac{[C_{dye}]_t}{[C_{dye}]_0} = e^{-kt} \tag{7}$$

$$[C_{dye}]_t = [C_{dye}]_o e^{-kt} \tag{8}$$

Results and discussion

Characterization

The phase identification and crystalline nature of fabricated g-C_3N_4-CuO-ZnO was confirmed using XRD. Figure 1 displays the XRD results. The existence of sharp peaks in the XRD pattern shows the crystalline nature of the g-C_3N_4-CuO-ZnO. The occurrence of g-C_3N_4 in the synthesized sample is verified by the presence of peaks at ~13° and 27° indicating (100) and (002) planes. The diffraction peaks at 2θ ~24° and at 2θ ~43° also represent the graphitic nature of the sample[38]. The diffraction peaks observed at ~36°, 39°, 49°, 54°, 58°, 62°, and 75° correspond to (111), (111), (202), (020), (202), (113), and (004) planes of the monoclinic structure of CuO (JCPDS: 01-080-1268). The diffraction peaks at 2θ ~32°, 34°, 36°, 48°, 57°, 63°, and 68° are characteristic peaks of wurtzite hexagonal phase of ZnO (JCPDS: 01-089-0510). These diffraction peaks correspond to (100), (002), (101), (102), (110), (103), and (112) planes, respectively[39–43]. A small shift in peak positions with respect to the standard XRD pattern is due to the doping of metal ions[44].

Functional groups were identified based on the FTIR spectrum (Fig. 2). The spectrum is dominated by several strong bands within the 1,060–1,700 cm^{-1} region such as 1,235, 1,316, 1,419, 1,574, 1,634, and 1,700 cm^{-1}. These are the representative peaks of stretching vibration of C=N and C–N functional groups associated with aromatic heterocycles. Similarly, the peaks observed at approximately 3,256 cm^{-1} are associated to the stretching of NH_2 groups or water molecules. The presence of a peak at 439 cm^{-1} represents the Zn-O linkage. Similarly, the peak at 608 cm^{-1} indicates the Cu-O bond. The absorption observed at 498 cm^{-1} confirms the attachment of CuO with ZnO particles[45–49]. Hence, the FTIR shows that the synthesized substance consists of g-C_3N_4, CuO, and ZnO.

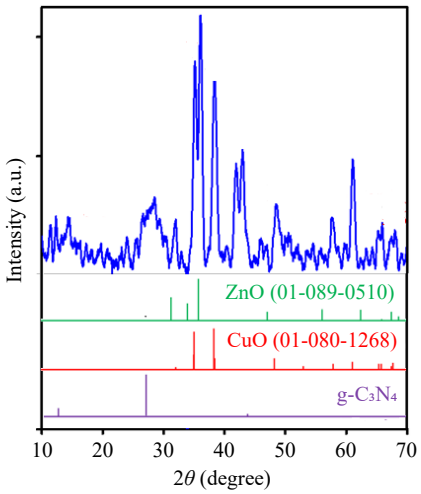

Fig. 1 XRD patterns of the g-C_3N_4-CuO-ZnO heterojunction.

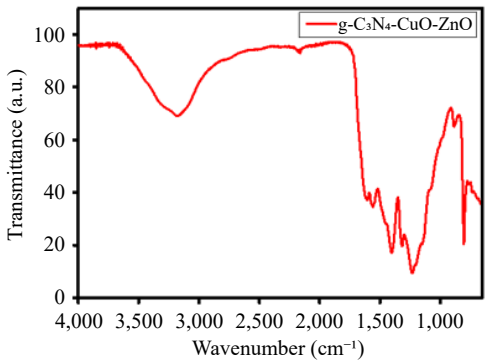

Fig. 2 FTIR spectrum of the g-C_3N_4-CuO-ZnO heterojunction.

The morphology and microstructure of g-C_3N_4-CuO-ZnO were studied by SEM. Figure 3 displays the SEM of g-C_3N_4-CuO-ZnO. It can be observed that the synthesized g-C_3N_4-CuO-ZnO exhibits a foam-like structure. This foam-like structure is due to the sheets of exfoliated g-C_3N_4. These sheets contribute to an enhanced surface area of the composites. It can also be observed that the morphology of synthesized g-C_3N_4-CuO-ZnO is uniform. This uniform morphology suggests the tight incorporation of CuO and ZnO in a sheet of g-C_3N_4. This structure favors the absorption of light which enhances the photocatalytic performance[38].

Thermal characteristics of synthesized substance were investigated by TGA and DTA. Figure 4 displays the mass change when the g-C_3N_4-CuO-ZnO heterojunction sample was exposed to heat treatment. From the TGA curve of the g-C_3N_4-CuO-ZnO heterojunction, a weight loss of about 30% was observed up to 400 °C. Similarly, the DTA shows a broad endothermic peak over the same temperature range. This change in TGA and DTA with temperature is attributed to the loss of adsorbed water.

Photocatalysis

The photocatalytic activity associated with synthesized g-C_3N_4-CuO-ZnO was studied through the degradation of selected dyes in sunlight. A 50 mL dye solution of crystal violet (CV)/methyl orange (MO) of 100 mg/L was used as a representative pollutant. For comparison, the degradation of both dyes was studied over individual g-C_3N_4, CuO, and ZnO as well in identical experimental conditions. Figure 5 displays the results of degradation of dyes with g-C_3N_4-CuO-ZnO, g-C_3N_4, CuO, and ZnO. It was noticed that about

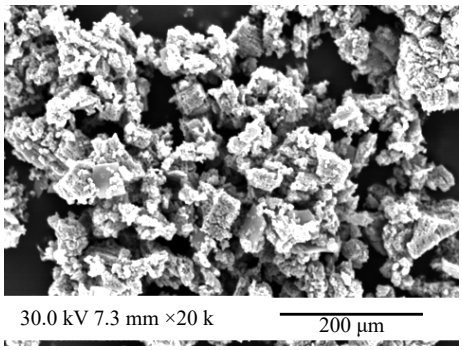

Fig. 3 SEM analysis of the g-C_3N_4-CuO-ZnO heterojunction.

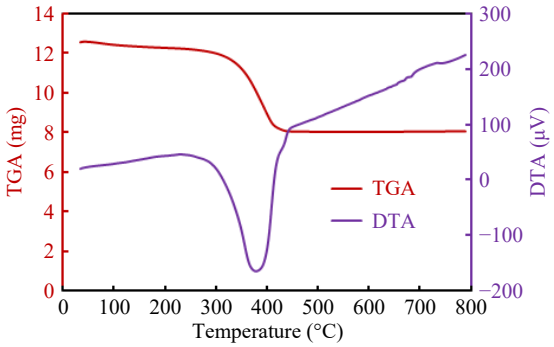

Fig. 4 TGA and DTA curves for the g-C_3N_4-CuO-ZnO heterojunction.

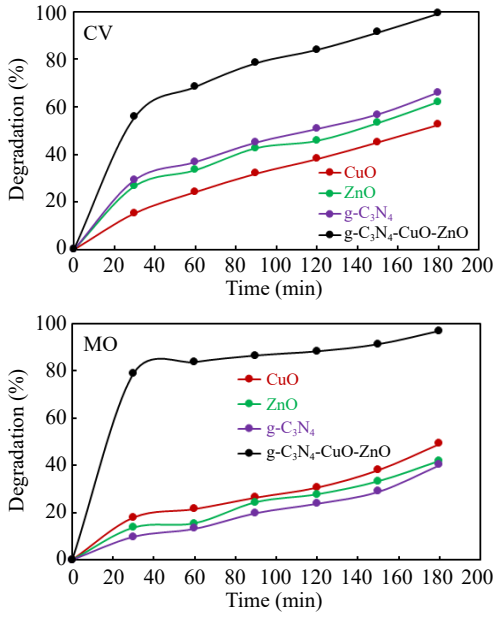

Fig. 5 Comparison of photocatalytic activities of different substances.

97%, 40%, 49%, and 42% of methyl orange degraded in the presence of g-C_3N_4-CuO-ZnO, g-C_3N_4, CuO, and ZnO during 180 min of reaction duration, respectively. Similarly, about 99%, 65%, 52%, and 62% of crystal violet dye degraded in the presence of g-C_3N_4-CuO-ZnO, g-C_3N_4, CuO, and ZnO during 180 min of reaction duration, respectively. It is evident that synthesized g-C_3N_4-CuO-ZnO is more effective in the photodegradation of methyl orange and crystal violet dyes. Furthermore, the data given in Fig. 5 indicates that the rate of degradation of dyes was highly accelerated at the beginning of the reaction and then decreased with the passage of time. During the start of the reaction, more hydroxyl radicals were produced

because of the abundance of catalyst active sites. With the passage of time, the catalyst active sites were occupied with different molecules, causing a retardation effect on the rate of reaction. Additionally, the degradation of dyes produces intermediate products that compete with the dye molecules for the degradation[50].

The kinetic Eqn (8) was applied to the degradation data given in Fig. 5 for kinetics analyses. The exponential equation was applied to the data using Solver of Excel software. Figure 6 shows the application of the kinetics model to the experimental data. The close agreement of the experimental and kinetics model predicted data shows that photocatalytic degradation of methyl orange and crystal violet dye follows the 1st order reaction kinetics. The 1st order rate constants were determined and are given in Table 1.

The pH of the reaction mixture is an important parameter that significantly affects photocatalytic activity. Therefore, the dependence of photocatalytic activity on pH was also explored. For this purpose, photodegradation of methyl orange and crystal violet dyes was studied over g-C_3N_4-CuO-ZnO photocatalyst at different pH from pH 3 to 11. A 100 mg/L dye solution was used for this study. A 0.05g of g-C_3N_4-CuO-ZnO was used as catalyst dosage. The pH of the reaction mixture was adjusted using a 0.1 M solution of HCl and NaOH. The reaction duration was 180 min. The results obtained are displayed in Fig. 7. The synthesized g-C_3N_4-CuO-ZnO showed the best catalytic performance at pH 11. The hydroxyl radicals are involved in the degradation of organic molecules. The higher concentration of hydroxyl ions at high pH facilitates the production of hydroxyl radicals, therefore, g-C_3N_4-CuO-ZnO exhibited the best catalytic performance under alkaline conditions[51].

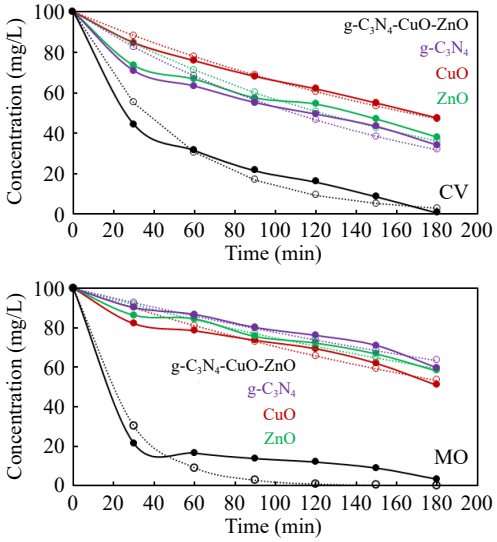

Fig. 6 Kinetics analysis of photocatalytic degradation data of dyes according to kinetics model given in Eqn (8). The solid lines represented the experimental data while the broken lines represent the data calculated by kinetics Eqn (8) using Solver.

Table 1. Rate constants for degradation of crystal violet and methyl orange dyes over different substances. These rate constants were determined by analyzing the degradation data according to kinetics Eqn (8) using Solver.

Catalyst	Crystal violet dye		Methyl orange dye	
	k (min^{-1})	R^2	k (min^{-1})	R^2
g-C_3N_4	0.00637	0.988	0.00252	0.986
CuO	0.00418	0.986	0.00349	0.987
ZnO	0.00568	0.988	0.00290	0.988
g-C_3N_4-CuO-ZnO	0.01978	0.947	0.03994	0.928

The dependence of catalytic activity on catalyst dosage was also explored by performing degradation experiments using 0.13, 0.05, 0.1, and 0.15 g of catalyst dosages. The optimum catalyst dosage was found to be 0.05 g of g-C_3N_4-CuO-ZnO. Similarly, the effect of hydrogen peroxide on the activity of g-C_3N_4-CuO-ZnO was also explored. It did not affect significantly the catalytic performance of synthesized g-C_3N_4-CuO-ZnO.

Photocatalytic mechanism

The exceptional performance of synthesized ternary g-C_3N_4-CuO-ZnO in the degradation of selected dyes is due to two reasons: (1) its ability of light harvesting; and (2) its ability to transfer the charges. The conduction band potential (on normalized hydrogen electrode (NHE)) of g-C_3N_4, CuO, and ZnO are −1.13, 0.65, and −0.30 eV, respectively. Similarly, the valence band potential of g-C_3N_4, CuO, and ZnO are 1.57, 1.97, and 2.88 eV, respectively[52,53]. Hence, an S-scheme photocatalytic mechanism can be established for charge separation on the basis of this information. Figure 8 explains the formation of the equilibrium of Fermi levels on g-C_3N_4-CuO-ZnO heterostructure. The absorption of photons excites the photocatalyst and generates e^-/h^+ pairs in the CB and VB of photocatalyst[54]. The CB of g-C_3N_4 is more negative than that of CuO and ZnO. Therefore, the photo-generated e^- in CB of g-C_3N_4 transfers to the CB of CuO. Meanwhile, the e^- induced in the CB of ZnO also moves into the CB of CuO. Furthermore, these electrons may also flow to the VB of g-C_3N_4 and ZnO, based on the S-scheme[55,56]. The CuO in g-C_3N_4-CuO-ZnO heterostructure serves as locations for recombination of photo generated e^- that decreases the migration of photo-generated e^-. Hence, the CuO in g-C_3N_4-CuO-ZnO serves as an electron acceptor from both g-C_3N_4 and ZnO resulting in the inhibition of recombination of e^-/h^+ pairs. As a result, the S-scheme enhances the separation of e^-/h^+ and preserves its high photo-redox

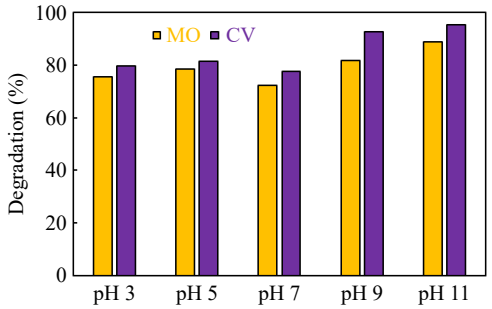

Fig. 7 Effect of initial pH on g-C_3N_4-CuO-ZnO catalyzed photodegradation of methyl orange and crystal violet dye.

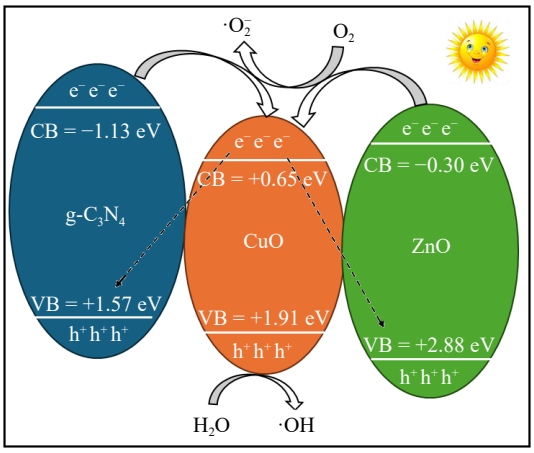

Fig. 8 Proposed mechanism of the photocatalytic process.

capability[57–59]. Similarly, has a higher valence band potential than g-C_3N_4 and a lower valence band potential of ZnO, therefore the photogenerated e^- is inclined to combination with h^+ in the valence band of CuO. Overall, the synthesized g-C_3N_4-CuO-ZnO exhibits enhanced photocatalytic performance due to reduced electron-hole recombination and improved charge separation[60–62].

Conclusions

The present study successfully synthesized and characterized a g-C_3N_4-CuO-ZnO heterojunction, demonstrating remarkable photocatalytic efficiency in degrading methyl orange (MO) and crystal violet (CV) dyes under sunlight irradiation. The integration of g-C_3N_4 with CuO and ZnO significantly enhanced the photocatalytic activity due to improved charge separation and light-harvesting ability. The heterojunction achieved degradation efficiencies of 96.84% for MO and 99.26% for CV within 180 min, outperforming the individual components. The investigation into various parameters, including pH, catalyst dosage, oxidant presence, and recycling of catalyst further highlighted the robustness and adaptability of the synthesized photocatalyst across diverse conditions. The proposed S-scheme mechanism underscores the role of CuO as an electron mediator, effectively reducing electron-hole recombination, and enhancing redox reactions. These findings pave the way for the development of effective and affordable photocatalysts for wastewater treatment, addressing environmental pollution through sustainable means. Future research could focus on scaling up the synthesis process and exploring the degradation of complex industrial effluents to broaden the application scope of this heterojunction.

Author contributions

The authors confirm contribution to the paper as follows: study conception and design: Saeed M; data collection: Pervaiz S, Khan I; analysis and interpretation of results: Saeed M, Jamal MA, Haq A, Javed M; draft manuscript preparation: Pervaiz S; revision and resources: Habila MA, Khan I. All authors reviewed the results and approved the final version of the manuscript.

Data availability

All data generated or analyzed during this study are included in this published article.

Acknowledgments

This work was funded by the Researchers Supporting Project Number (RSP2025R441), King Saud University, Riyadh, Saudi Arabia.

Conflict of interest

The authors declare that they have no conflict of interest.

Dates

Received 25 December 2024; Revised 3 April 2025; Accepted 22 April 2025; Published online 6 June 2025

References

1. Sheng J, Cheng Q, Yang H. 2024. Water markets and water inequality: China's water rights trading pilot. *Socio-Economic Planning Sciences* 94:101929
2. Zhang Y, Liu Z, Wang J, Du H, Sun Q, et al. 2025. Efficient and high-selective lithium extraction from waste $LiMn_2O_4$ batteries by synergetic pyrolysis with polyvinyl chloride. *Waste Management* 198:95–105
3. Iqbal MS, Aslam AA, Iftikhar R, Junaid M, Imran SM, et al. 2023. The potential of functionalized graphene-based composites for removing heavy metals and organic pollutants. *Journal of Water Process Engineering* 53:103809
4. Li X, Shi XL, Wang J, Shi K, Wang Q. 2024. Effect of different hydrogen donors on the catalytic conversion of levulinic acid to γ-valerolactone over non-noble metal catalysts. *Journal of Industrial and Engineering Chemistry* 138:17–33
5. Ni ZL, Ma JS, Liu Y, Li BH, Nazarov AA, Li H. et al. 2025. Numerical analysis of ultrasonic spot welding of Cu/Cu joints. *Journal of Materials Engineering and Performance*
6. Karthik TVK, Maldonado A, de la L Olvera M, Hernández AG, Vega-Pérez J, et al. 2021. Copper-doped ZnO thin films deposited by spray pyrolysis: effect of water content in starting solution on methylene blue degradation by Photocatalysis. *Journal of Electronic Materials* 50:5542–52
7. Yadav K, Datta D, Jana B. 2024. Enhanced photocatalytic degradation of Reactive Green 19 dye using earthworms like T-ZnO-CuO nano-composite material as a S-scheme heterojunction photocatalyst. *Inorganic Chemistry Communications* 170:113165
8. Yao Y, Yu L, Ghogare R, Dunsmoor A, Davaritouchaee M, et al. 2017. Simultaneous ammonia stripping and anaerobic digestion for efficient thermophilic conversion of dairy manure at high solids concentration. *Energy* 141:179–88
9. Yao Y, Zhou J, An L, Kafle GK, Chen S, et al. 2018. Role of soil in improving process performance and methane yield of anaerobic digestion with corn straw as substrate. *Energy* 151:998–1006
10. Bi F, Zhou B, Li R, Du R, Zheng Z, et al. 2024. One-step electrospun $ZnFe_2O_4$/ZnO/CuO composite photo-Fenton nanofibers for efficient degradation of organic dyes. *Materials Today Communications* 41:11066
11. Wang Z, Lu D, Kondamareddy KK, He Y, Gu W, et al. 2024. Recent advances and insights in designing Zn_xCd1-_xS-based photocatalysts for hydrogen production and synergistic selective oxidation to value-added chemical production. *ACS Applied Materials & Interfaces* 16(37):48895–926
12. Kossar S, Shameem Banu IB, Aman N, Amiruddin R. 2021. Investigation on photocatalytic degradation of crystal violet dye using bismuth ferrite nanoparticles. *Journal of Dispersion Science and Technology* 42(14):2053–62
13. Jiang X, Yang Z, Li W, Liu J, Zhang D, et al. 2023. Thorny hydrangea-like $SnIn_4S_8/Mn_{0.3}Cd_{0.7}S$ as novel type-II heterojunction photocatalyst to enhance the efficient degradation of imidacloprid. *Applied Surface Science* 617:56632
14. Oyetade JA, Machunda RL, Hilonga A. 2022. Photocatalytic degradation of azo dyes in textile wastewater by Polyaniline composite catalyst-a review. *Scientific African* 17:e01305
15. Zhao D, Wang Y, Dong CL, Huang YC, Chen J, et al. 2021. Boron-doped nitrogen-deficient carbon nitride-based Z-scheme heterostructures for photocatalytic overall water splitting. *Nature Energy* 6(4):388–397
16. Yao Y, Chen S. 2016. A novel and simple approach to the good process performance of methane recovery from lignocellulosic biomass alone. *Biotechnology for Biofuels* 9:115
17. Gao L, Cao M, Zhang C, Li J, Zhu X, et al. 2024. Zinc selenide/cobalt selenide in nitrogen-doped carbon frameworks as anode materials for high-performance sodium-ion hybrid capacitors. *Advanced Composites and Hybrid Materials* 7(5):144
18. Yao Y, Chen S, Kafle GK. 2017. Importance of "weak-base" poplar wastes to process performance and methane yield in solid-state anaerobic digestion. *Journal of Environmental Management* 193:423–29
19. Yao Y, He M, Ren Y, Ma L, Luo Y, et al. 2013. Anaerobic digestion of poplar processing residues for methane production after alkaline treatment. *Bioresource Technology* 134:347–52
20. Akter J, Sapkota KP, Hanif MA, Islam MA, Abbas HG, et al. 2021. Kinetically controlled selective synthesis of Cu_2O and CuO nanoparticles toward enhanced degradation of methylene blue using ultraviolet and sunlight. *Materials Science in Semiconductor Processing* 123:105570

21. Qamar MA, Shahid S, Javed M, Iqbal S, Sher M, et al. 2021. Designing of highly active g-C_3N_4/Ni-ZnO photocatalyst nanocomposite for the disinfection and degradation of the organic dye under sunlight radiations. *Colloids and Surfaces A: Physicochemical and Engineering Aspects* 614:126176
22. Vakili B, Shahmoradi B, Maleki A, Safari M, Yang J, et al. 2019. Synthesis of immobilized cerium doped ZnO nanoparticles through the mild hydrothermal approach and their application in the photodegradation of synthetic wastewater. *Journal of Molecular Liquids* 280:230–37
23. Arshad M, Qayyum A, Abbas G, Haider R, Iqbal M, et al. 2018. Influence of different solvents on portrayal and photocatalytic activity of tin-doped zinc oxide nanoparticles. *Journal of Molecular Liquids* 260:272–78
24. Nguyen LTT, Nguyen LTH, Duong ATT, Nguyen BD, Hai NQ, et al. 2019. Preparation, characterization and photocatalytic activity of La-doped zinc oxide nanoparticles. *Materials* 12(8):1195
25. Babajani N, Jamshidi S. 2019. Investigation of photocatalytic malachite green degradation by iridium doped zinc oxide nanoparticles: Application of response surface methodology. *Journal of Alloys and Compounds* 782:533–44
26. Liu J, Jin J, Deng Z, Huang SZ, Hu ZY. et al. 2012. Tailoring CuO nanostructures for enhanced photocatalytic property. *Journal of Colloid and Interface Science* 384:1–9
27. Senthil Kumar P, Selvakumar M, Ganesh Babu S, Induja S, Karuthapandian S. 2017. CuO/ZnO nanorods: an affordable efficient p-n heterojunction and morphology dependent photocatalytic activity against organic contaminants. *Journal of Alloys and Compounds* 701:562–573
28. Gu W, Lu D, Kondamareddy KK, Li J, Cheng P, et al. 2024. Efficient photocatalytic decomposition of NO and mechanism insight enabled by $NaBH_4$-reduced N(ligancy-3)-vacancy-rich-graphitic carbon nitride. *Materials Today Physics* 46:101487
29. Alhashmialameer D, Shariq M, Qamar MA, Althikrallah HA, Al-Qasmi N. et al. 2025. Improved catalytic performance of (Fe, Cr)-ZnO/g-C3N4 nanocomposite towards electrocatalytic water splitting for clean energy. *Solid State Sciences* 160:107823
30. Zheng Y, Liu Y, Guo X, Chen Z, Zhang W, et al. 2020. Sulfur-doped g-C_3N_4/rGO porous nanosheets for highly efficient photocatalytic degradation of refractory contaminants. *Journal of Materials Science & Technology* 41:117–26
31. Su Y, Shen Z, Long X, Chen C, Qi L, et al. 2023. Gaussian filtering method of evaluating the elastic/elasto-plastic properties of sintered nanocomposites with quasi-continuous volume distribution. *Materials Science and Engineering: A* 872:145001
32. Tian J, Zhong K, Zhu X, Yang J, Mo Z, et al. 2023. Highly exposed active sites of Au nanoclusters for photocatalytic CO_2 reduction. *Chemical Engineering Journal* 451:138392
33. Shariq M, Alshehri K, Mohammed Bouzgarrou S, Kashif Ali S, Alqurashi Y, et al. 2024. Progress in development of MXene-based nanocomposites for Supercapacitor application - a review. *FlatChem* 44:100609
34. BaQais A, Shariq M, Almutib E, Al-Qasmi N, Azooz RE, et al. 2023. NiO and magnetic $CuFe_2O_4$-based composite electrocatalyst for enhanced oxygen evolution reaction. *The European Physical Journal Plus* 138(9):1–9
35. Siddique M, Khan NM, Saeed M, Ali S, Shah Z. 2021. Green synthesis of cobalt oxide nanoparticles using Citrus medica leaves extract: characterization and photo-catalytic activity. *Zeitschrift Fur Physikalische Chemie* 235(6):663–68
36. Nisar A, Saeed M, Usman M, Muneer M, Adeel M, et a. 2020. Kinetic modeling of ZnO-rGO catalyzed degradation of methylene blue. *International Journal of Chemical Kinetics* 52(10):645–54
37. Zhang Y, Xu L, Wang J, Pan H, Dou M. et al. 2025. Bagasse-based porous flower-like MoS_2/carbon composites for efficient microwave absorption. *Carbon Letters* 35:145–60
38. Saeed M, Asghar HA, Khan I, Akram N, Usman M. 2025. Synthesis of TiO_2-g-C_3N_4 for efficient photocatalytic degradation of Congo Red dye. *Catalysis Today* 447:115154
39. Sivasakthi S, Gurunathan K. 2020. Graphitic carbon nitride bedecked with CuO/ZnO hetero-interface microflower towards high photocatalytic performance. *Renewable Energy* 159:786–800
40. Lam SM, Sin JC, Mohamed AR. 2016. A review on photocatalytic application of g-C_3N_4/semiconductor (CNS) nanocomposites towards the erasure of dyeing wastewater. *Materials Science in Semiconductor Processing* 47:62–84
41. Sathishkumar P, Sweena R, Wu JJ, Anandan S. 2011. Synthesis of CuO-ZnO nanophotocatalyst for visible light assisted degradation of a textile dye in aqueous solution. *Chemical Engineering Journal* 171:136–40
42. Gajendiran J, Rajendran V. 2014. Synthesis and characterization of coupled semiconductor metal oxide (ZnO/CuO) nanocomposite. *Materials Letters* 116:311–13
43. Chitralekha, Maurya I, Gupta T, Shankar S, Gaurav S, et al. 2022. Dielectric and impedance studies of binary ZnO–CuO nanocomposites for hydroelectric cell application. *Materials Chemistry and Physics* 291:126690
44. Saeed M, Khan I, Adeel M, Akram N, Muneer M. 2022. Synthesis of a CoO–ZnO photocatalyst for enhanced visible-light assisted photodegradation of methylene blue. *New Journal of Chemistry* 46:2224
45. Cahino AM, Loureiro RG, Dantas J, Madeira VS, Ribeiro Fernandes PC. 2019. Characterization and evaluation of ZnO/CuO catalyst in the degradation of methylene blue using solar radiation. *Ceramics International* 45(11):13628–36
46. Song J, Wang X, Ma J, Wang X, Wang J, et al. 2018. Visible-light-driven in situ inactivation of *Microcystis aeruginosa* with the use of floating g-C_3N_4 heterojunction photocatalyst: performance, mechanisms and implications. *Applied Catalysis B: Environmental* 226:83–92
47. He B, Feng M, Chen X, Zhao D, Sun J. 2020. One-pot construction of chitin-derived carbon/g-C_3N_4 heterojunction for the improvement of visible-light photocatalysis. *Applied Surface Science* 527:146737
48. Han H, Ding G, Wu T, Yang D, Jiang T, et al. 2015. Cu and boron doped carbon nitride for highly selective oxidation of toluene to benzaldehyde. *Molecules* 20:12686–97
49. Das S, Srivastava VC. 2017. Synthesis and characterization of ZnO/CuO nanocomposite by electrochemical method. *Materials Science in Semiconductor Processing* 57:173–177
50. Shinde RS, Khairnar SD, Patil MR, Adole VA, Koli PB, et al. 2022. Synthesis and characterization of ZnO/CuO nanocomposites as an effective photocatalyst and gas sensor for environmental remediation. *Journal of Inorganic and Organometallic Polymers and Materials* 32:1045–66
51. Kumaresan N, Sinthiya MMA, Ramamurthi K, Ramesh Babu R, Sethuraman K. 2020. Visible light driven photocatalytic activity of ZnO/CuO nanocomposites coupled with rGO heterostructures synthesized by solid-state method for RhB dye degradation. *Arabian Journal of Chemistry* 13:3910–28
52. Rajendran R, Vignesh S, Suganthi S, Raj V, Kavitha G, et al. 2022. g-C_3N_4/TiO_2/CuO S-scheme heterostructure photocatalysts for enhancing organic pollutant degradation. *Journal of Physics and Chemistry of Solids* 161:110391
53. Abbasi E, Haghighi M, Shabani M, Niyati A, Mahboob S. 2023. Boosted ultrasound-sunlight-driven removal of organic pollutant over double Z-scheme plasmonic ZnO–Cu–CuO/g-C_3N_4 nanophotocatalyst: design via in-situ co-precipitation hybrid with various sonication powers. *Materials Today Sustainability* 24:100580
54. Huang FP, Qin WJ, Pan XY, Yang K, Wang K, et al. 2024. Visible-light-induced chemodivergent synthesis of tetracyclic quinazolinones and 3-iminoisoindoliones via the substrate control strategy. *The Journal of Organic Chemistry* 89(7):4395–405
55. Zhao Z, Zhang W, Shen X, Muhmood T, Xia M, et al. 2018. Preparation of g-C_3N_4/TiO_2/$BiVO_4$ composite and its application in photocatalytic degradation of pollutant from TATB production under visible light irradiation. *Journal of Photochemistry and Photobiology A: Chemistry* 358:246–55
56. Vosoughi F, Habibi-Yangjeh A, Asadzadeh-Khaneghah S, Ghosh S, Maiyalagan T. 2020. Novel ternary g-C_3N_4 nanosheet/Ag_2MoO_4/AgI photocatalysts: impressive photocatalysts for removal of various contaminants. *Journal of Photochemistry and Photobiology A: Chemistry* 403:112871
57. Wageh S, Al-Ghamdi AA, Jafer R, Li X, Zhang P. 2021. A new heterojunction in photocatalysis: S-scheme heterojunction. *Chinese Journal of Catalysis* 42:667–69
58. Xu Q, Zhang L, Cheng B, Fan J, Yu J. 2020. S-scheme heterojunction photocatalyst. *Chem* 6:1543–59

59. Balu S, Velmurugan S, Palanisamy S, Chen SW, Velusamy V, et al. 2019. Synthesis of α-Fe_2O_3 decorated g-C_3N_4/ZnO ternary Z-scheme photocatalyst for degradation of tartrazine dye in aqueous media. *Journal of the Taiwan Institute of Chemical Engineers* 99:258–67
60. Van KN, Nguyen Thi VN, Tran Thi TP, Truong TT, Lieu Le Thi T, et al. 2020. A novel preparation of GaN-ZnO/g-C_3N_4 photocatalyst for methylene blue degradation. *Chemical Physics Letters* 763:138191
61. Xie Q, He W, Liu S, Li C, Zhang J, et al. 2020. Bifunctional S-scheme g-C_3N_4/Bi/$BiVO_4$ hybrid photocatalysts toward artificial carbon cycling. *Chinese Journal of Catalysis* 41:140–53
62. Obregón S, Zhang Y, Colón G. 2016. Cascade charge separation mechanism by ternary heterostructured $BiPO_4$/TiO_2/g-C_3N_4 photocatalyst. *Applied Catalysis B Environmental* 184:96–103